[Technical Paper]

Study on Electrostatic Inchworm Motor Device for a Heterogeneous Integrated Microrobot System

Ken Saito*,**, Daniel S. Contreras**, Yudai Takeshiro***, Yuki Okamoto***, Satoshi Hirao*, Yuya Nakata*, Taisuke Tanaka*, Satoshi Kawamura*, Minami Kaneko*, Fumio Uchikoba*, Yoshio Mita***, and Kristofer S. J. Pister**

**Nihon University, 7-24-1, Narashinodai, Funabashi-shi, Chiba 274-8501, Japan*

***University of California, Berkeley, CA 94720, USA*

****The University of Tokyo, 7-3-1 Hongo, Bunkyo-ku, Tokyo 113-8656, Japan*

(Received August 27, 2018; accepted December 26, 2018, published April 2, 2019)

Abstract

Ideal microrobots are on the millimeter-scale with integrated actuators, power sources, sensors, and controllers. Numerous researchers are inspired by insects for the mechanical or electrical design of microrobots. Previously, the authors proposed and demonstrated microrobots that can replicate the tripod gait locomotion of an ant, the legs of which were actuated by shape memory alloy (SMA) actuators. The SMA provided a large deformation and force, but the power consumed by actuating a single leg reached as high as 94 mW. This paper discusses a silicon electrostatic inchworm motor chip to move a robot leg with low energy consumption using a small power source. The inchworm motor chip was actuated by electrostatic motors. The power consumption was as low as 1.0 mW, in contrast with SMA actuators. The reciprocal motion of the inchworm motor chip is powered by silicon photovoltaic cells. The results show that the 7.5 mm^2 photovoltaic cells could produce 60 V to actuate the inchworm motor chip, and the generated force is enough to move the leg of the microrobot. Thus, we demonstrated the actuation of a microrobot leg using an electrostatic inchworm motor chip, which is the first reported instance of an electrostatic motor driving an off-chip structure.

Keywords: Heterogeneous Integration, Silicon Device, Microrobot, Electrostatic Motor, Inchworm Motor Chip, Photovoltaic Cells

1. Introduction

Several microrobot systems ranging in scale from micrometers to centimeters have been demonstrated. [1–12] Among these microrobots, the micrometer-scale ones have potential applications in special environments such as surgery inside the narrow blood vessels of the human brain or microassembly for small mechanical systems.[4, 8] However, adding power sources and controllers into microscale systems is difficult. Therefore, passive control schemes using external electrical or magnetic forces are commonly implemented. A number of centimeter-scale robots have been constructed from miniaturized electrical components integrated with sensors, actuators, power sources, and controllers,[6, 9] and several bio-inspired robots have been proposed. In particular, the locomotion mechanisms of insects have attracted the attention of researchers.[5, 7] However, millimeter-scale robots do not behave like insects because of the difficulty in integrating power sources and actuators onto the robot.[13, 14] In seeking further miniaturization, some researchers have used microfabrication technology to fabricate small actuators.[15, 16] Some examples include piezoelectric actuators, shape memory alloy (SMA) actuators, electrostatic actuators, and ion-exchange polymer actuators. These actuators offer different advantages such as power consumption, switching speed, force generation, displacement, and ease of fabrication. In general, an actuator can only generate either rotary or linear motion, and mechanical mechanisms are necessary to convert the movements generated by the actuators into locomotion.

Previously, the authors demonstrated a millimeter-scale hexapod-type microrobot to perform the tripod gait loco-

motion of an ant [17] and a quadruped-type microrobot to replicate the quadrupedal gait locomotion of an animal [18] by using SMA actuators to provide a large deformation and a large force. This paper discusses an electrostatic inchworm motor chip [19–21] that consumes low energy and uses a small power source. The leg of the microrobot is designed to allow reciprocal motions and is powered by silicon photovoltaic (hereafter, PV) cells.[22, 23]

2. High-Voltage Silicon PV Cells

Figure 1 shows the fabricated high-voltage silicon PV cell array. The PV cell array was designed with an area of 7.5 mm^2. The device was constructed using a complementary metal-oxide-semiconductor (CMOS) postprocess dry release and device isolation method. The array consists of 144 PV cells connected in series, and each cell has a p-diffusion layer on an n-well. The design and process method are described in detail in references.[22, 23]

Figure 2 shows the current–voltage (I–V) characteristics of the PV cell array. The PV cell array was measured using a KEITHLEY 2000 MULTIMETER. The light source was a 54 light emitting diode (LED) array (6 W) with a 6 V DC voltage source. The open-circuit voltage (V_{OC}) was 69 V, from which we can deduce that the V_{OC} of each cell was about 0.48 V on average. The short-circuit current (I_{SC}) was 28 mA. I_{SC} depends on the light intensity; therefore, increasing the intensity of the light source will increase I_{SC}. The maximum power (P_{MAX}) was 1.1 mW, which occurred at a voltage of 50 V and a current of 22 mA.

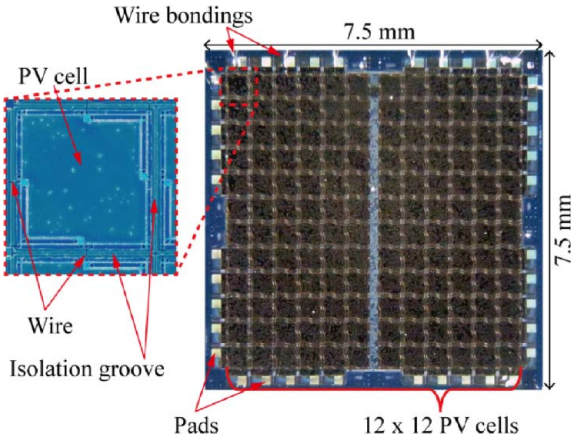

Fig. 1 High-voltage silicon PV cell array.

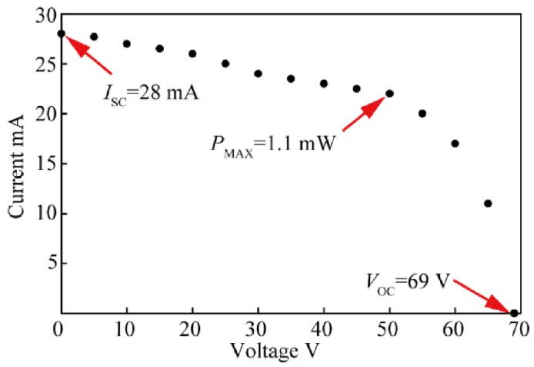

Fig. 2 I–V curve of silicon PV array.

3. Electrostatic Inchworm Motor Chip

As an alternative low-power means of actuation, electrostatic inchworm motors can be used to drive the legs of the microrobot. Micro electro mechanical systems (MEMS) electrostatic inchworm motors are based on capacitive driven gap-closing actuators (GCAs) working in tandem to linearly displace a shuttle at a force output of over 100 μN without any static current.[19]

Figure 3 shows an inchworm motor chip. The inchworm motor chip consists of a shuttle, a coupler, the main spring, subsprings, and GCAs. The shuttle is supported on the substrate by the main spring and subsprings. The coupler connects the chip to an off-chip structure. The GCAs have a fixed electrode, a movable electrode, a stopper, a spring, and an angled arm. The movable electrode is attached to the substrate by the spring, and the fixed electrode is directly fixed to the substrate. The stopper is attached to the movable electrode to avoid pulling in both electrodes. The authors used an angled arm design on the basis of work in reference.[20] In this design, the GCAs move an attached angled arm in an inchworm-like movement to impact a shuttle and push it in a preferential direction. The motors have a gap size of 1.6 μm, and each step of the motor moves the shuttle by 1.0 μm. Each GCA has 70 fingers, totaling 140 fingers for each actuation step. The inchworm motor chip measures a total area of approximately 2.2 mm × 2.5 mm. The electrostatic inchworm motors are fabricated in a three-mask silicon-on-insulator (SOI) pro-

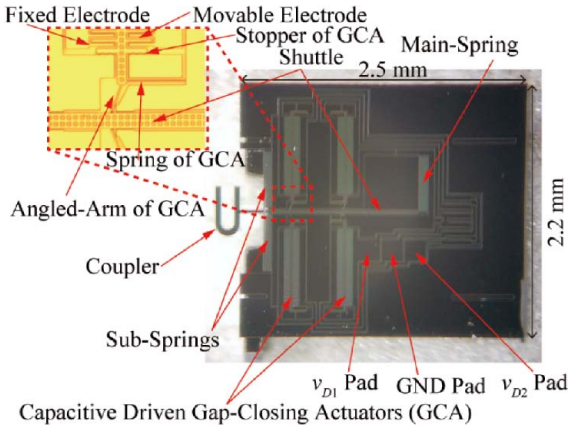

Fig. 3 Fabricated inchworm motor chip.

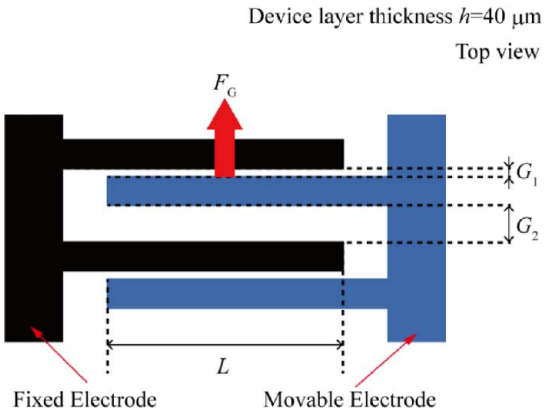

Fig. 4 Basic design of the capacitive driven GCAs.

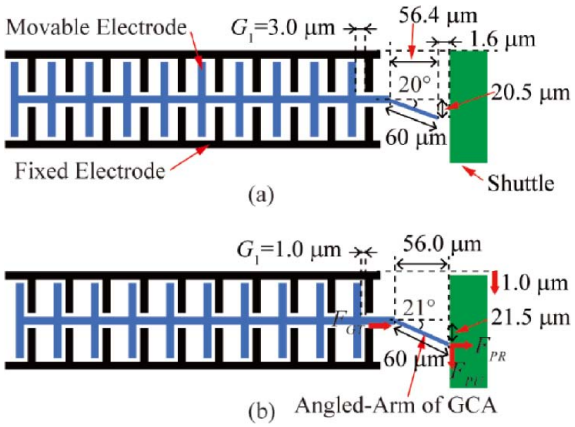

Fig. 5 Actuation method of the inchworm motor: (a) standard state (V = 0 V) and (b) active state (V = 60 V).

cess. The SOI wafers had a 40 μm device layer, 2 μm buried oxide, and a 550 μm handle wafer. A layer of 100-nm-thick aluminum is deposited on the device layer silicon to define the contact pads (v_{D1} Pad, v_{D2} Pad, and GND Pad). The device layer silicon is etched to form the structure of the motors using deep reactive-ion etching (DRIE). The back is then etched to reduce the mass and release the single chip from the substrate.

Figure 4 shows the basic design of the GCA. The output force F_G of one pair of GCAs is given by the following equation:

$$F_G = \frac{\varepsilon h L}{2}\left(\frac{1}{G_1^2} - \frac{1}{G_2^2}\right)V^2 \quad (1)$$

where ε is the dielectric constant in air, h is the device layer thickness, L is the overlap length of electrodes, G is the distance between the movable and fixed electrodes, and V is the applied voltage. F_G is 31 μN in the case of $\varepsilon = 8.8 \times 10^{-12}$ F/m, h = 40 μm, L = 50 μm, G_1 = 1.0 μm, G_2 = 7.0 μm, and V = 60 V. Each GCA has 70 fingers; hence, the total force of the electrostatic motors F_{GT} is 2.2 mN.

Figure 5 shows the actuation method of the inchworm motor. Figure 5(a) shows the standard state (V = 0 V), and Fig. 5(b) shows the active state (V = 60 V). In the case of Fig. 5(a), G_1 = 3.0 μm, the distance between the leg and the shuttle is 1.6 μm, and the angle of the leg is 20°. In the case of Fig. 5(b), G_1 = 1.0 μm, the distance between the leg and the shuttle is 0 μm, and the angle of the leg is 21°. In other words, the 2.0 μm movement of the movable electrode will push the shuttle by 1.0 μm. The pressing force F_{PR} and the pushing force F_{PU} of the movable electrode on the shuttle can be derived from F_{GT}:

$$F_{PR} = F_{GT}\cos 21° = 2.0 \text{ mN} \quad (2)$$

$$F_{PU} = F_{GT}\sin 21° = 0.78 \text{ mN} \quad (3)$$

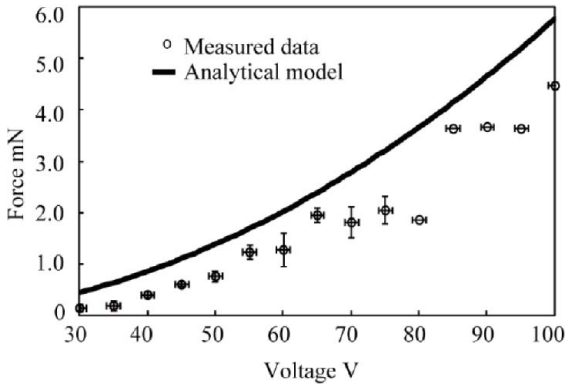

Fig. 6 Raw force output of the inchworm motor chip.

Figure 6 shows the force output of an electrostatic inchworm motor. The force is measured using a serpentine spring assembly with a spring constant of 0.067 N/m attached to the motor shuttle. The measured displacement of the inchworm shuttle can be related to the force output of the motor. The solid line highlights the analytical calculation of the force output. We can see that at 60 V, we attain an average force output of over 1 mN from 5 measured devices. The original angled arm inchworm motors shown in reference [20] were able to generate 1.9 mN at 110 V. Previous work has shown 0.50 mN of force at 60 V,[21] whereas the newly fabricated devices have demonstrated 1.3 mN of force at 60 V. Discrepancies between the analytical model and the measured values can be attributed to the unaccounted lateral etching of the silicon sidewalls, which can increase the effective finger gap size and change the spring constants.

4. Leg of the Microrobot System

Figure 7 shows the previous quadruped-type microrobot using SMA actuators.[18] Each leg of the robot can perform the stepping motion via a single actuator. In this work, the SMA actuator has been changed to electrostatic inchworm motors. The leg is fixed on both sides of the

body, and the number of legs of the microrobot can be easily increased. In this paper, the actuator connection part has been redesigned to accommodate the electrostatic inchworm motors.

Figure 8 shows the mechanical parts of the leg made from a silicon wafer, except for the shaft and steady pin. The shapes of the mechanical parts are machined using an inductively coupled plasma dry etching process with photolithography technology. The authors manually assembled the mechanical parts of the robot because constructing a complicated three-dimensional structure is difficult using microfabrication technology. During the process, 200-μm-thick silicon wafers were used for the mechanical parts except for the washer, which used 100-μm-thick silicon wafers. The shaft was constructed using cemented carbide to have a diameter of 0.1 ± 0.002 mm. The washer keeps each mechanical part fixed, and the washer and shaft were glued using cyanoacrylate. All the silicon parts have a clearance of 10 μm between the shafts to keep them movable. The stepping pattern of the microrobot is realized by 2 sets of four-bar linkages. Bars 1, 2, 3, and 4 are the primary (top) four-bar linkages, and bars 3, 4, 5, and 6 are the secondary (bottom) four-bar linkages. The primary and secondary sets of four-bar linkages are combined using bars 3 and 4 (Fig. 9).

Figure 10 shows the leg motion and trajectory. The origin coordinates (x_0, y_0) are the only points fixed to the body frame of the robot. The inflection point of the trajectory has 4 points: (x_1, y_1), (x_2, y_2), (x_3, y_3), and (x_4, y_4). The steady pin and the hole of bar 4 cause the inflection of the trajectory. The 4 points can be expressed by the difference between the angles of θ_α and θ_β. The difference between θ_α and θ_β can cause the reciprocal movement of point P. In other words, Fig. 10 shows that the designed leg can perform the stepping motion by the reciprocal movement of

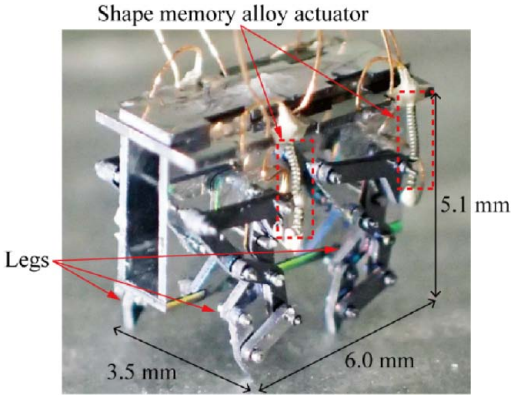

Fig. 7 Previous microrobot system using an SMA actuator.[18]

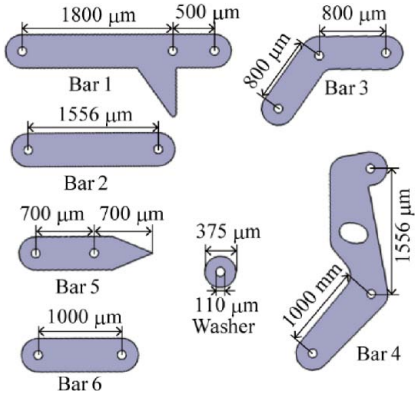

Fig. 8 Mechanical parts of the leg.

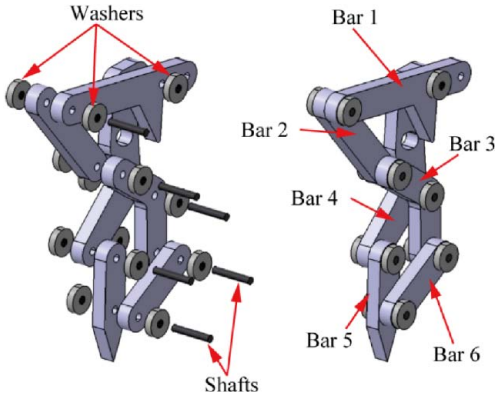

Fig. 9 Assembling method of the leg.

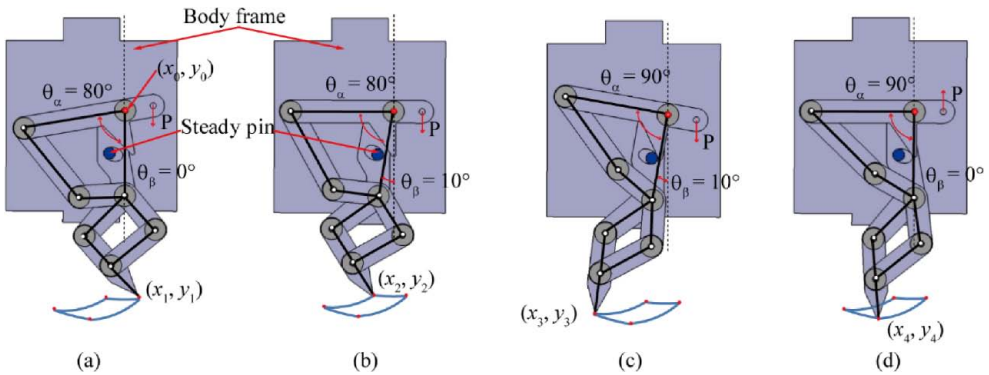

Fig. 10 Leg motion and trajectory of the leg: (a) (x_1, y_1), (b) (x_2, y_2), (c) (x_3, y_3), and (d) (x_4, y_4).

Table 1 Derived coordinates of each foot point.

Displacement of P (μm, actual)	Foot point	θ_α and θ_β	Coordinates (μm)
0 (0)	(x_1, y_1)	80° and 0°	(227.2, –3249.4)
87 (125)	(x_2, y_2)	80° and 10°	(–340.5, –3239.5)
174 (250)	(x_3, y_3)	90° and 10°	(–1248.6, –3440.3)
87 (125)	(x_4, y_4)	90° and 0°	(–632.3, –3604.9)

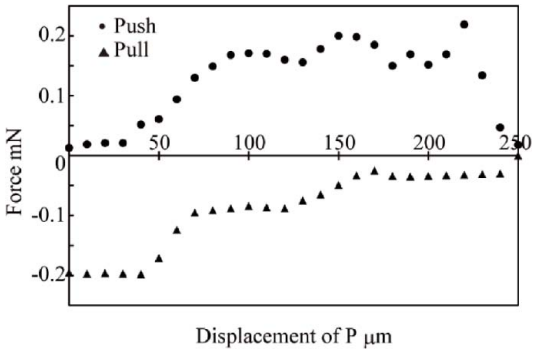

Fig. 11 Force required to actuate the leg.

point P.

Table 1 shows the derived coordinates of each foot point using the length between each joint of the leg (Fig. 10), θ_α and θ_β. In addition, the displacement of point P is described. The coordinates were derived using a trigonometric function. These results show that the designed leg can perform the stepping motion that is needed to move the quadruped-type microrobot.

Figure 11 shows the force required to actuate the leg. The abscissa shows the displacement of P, and the ordinate shows the required force to actuate the leg. The force was measured using a microforce sensor from Nano Control Co., Ltd., by fixing the microforce sensor to point P. This figure shows that a maximum force of 0.25 mN is required to move the leg from Fig. 10(a) to Fig. 10(c) (i.e., to push P), and a maximum of 0.20 mN is required to move the leg from Fig. 10(c) to Fig. 10(a) (i.e., to pull P). This result is measured horizontally instead of vertically, as shown in Fig. 7. The friction of each part differs with the direction. In the vertical condition, the push motion requires 0.54 mN, whereas the pull motion requires 0.36 mN.

5. Experimental Results

The anode side of the PV cell array was connected to a solid resistor at the collector of the transistor (Fig. 12(a)). In other words, the voltage generated by the PV cell, V_{PV},

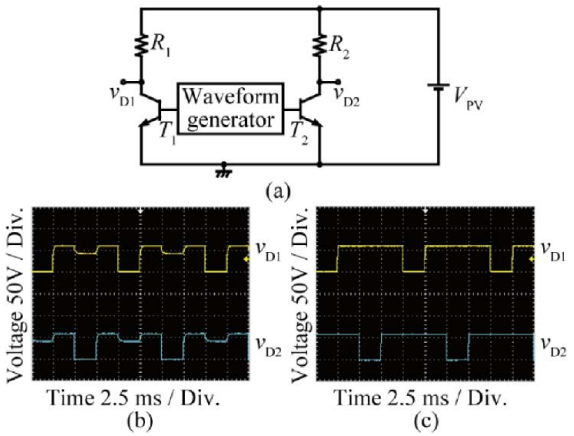

Fig. 12 Driver circuit of the inchworm motor chip. (a) Circuit diagram and examples of the driving waveform using (b) PV cells and (c) a voltage source.

was used as the voltage source of the circuit. A Fluke 280 waveform generator was used to switch the transistor (2N5550) and to generate the driving waveforms v_{D1} and v_{D2} for the inchworm motor chip. The driving waveforms were 2 offset 60 V amplitude 50 Hz square waves, one for each of the GCAs of the motor. The circuit constant was $R_1 = R_2 = 2.2$ MΩ. Figure 12(b) and 12(c) show an example of the driving waveform of the electrostatic inchworm motor. Figure 12(b) and 12(c) show the driving waveforms using a PV cell array and a voltage source, respectively. The driving waveform is a square wave with a pulse width of 10 ms, a pulse period of 7.5 ms, and a pulse amplitude of 60 V. Figure 12(b) shows the voltage drop in the middle of the square wave. The voltage drop will increase if R_1 and R_2 of the driver circuit are decreased. The voltage drop will also increase with a lower light intensity, which can be avoided using a higher-intensity light source (e.g., a xenon lamp). In addition, the inchworm motor chip can maintain the position of the shuttle in any timing by inputting the direct current voltage into v_{D1} and v_{D2}.

Figure 13 shows the actuation of the leg using electrostatic inchworm motors. The coupler attached to the shuttle of the electrostatic inchworm motors was connected to the leg through the shaft of point P. The result in Fig. 13 shows that the electrostatic inchworm motors produced a displacement of about 250 μm to move the leg of the microrobot. However, the pull motion was not enough to actuate the leg from (x_4, y_4) to (x_1, y_1) because the main spring and subspring were designed to generate a 0.05 mN pull motion, which is insufficient to complete the pull motion (completing the pull motion requires 0.20 mN). A pull motion using a spring structure is not realistic. Thus, the authors are planning to design a pair of inchworm

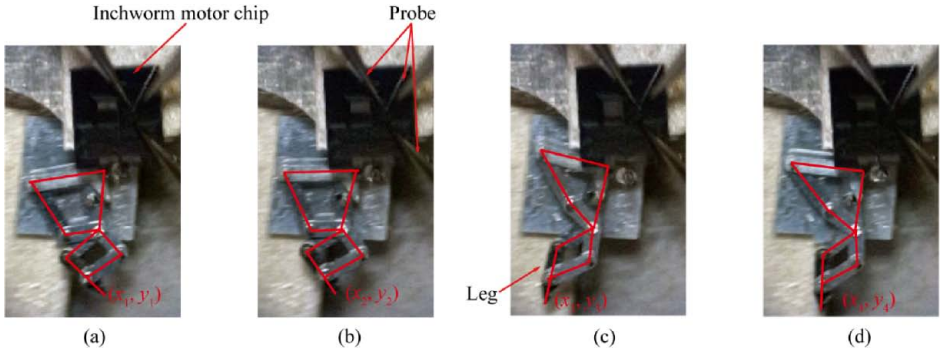

Fig. 13 Electrostatic inchworm motor for leg actuation: (a) (x_1, y_1), (b) (x_2, y_2), (c) (x_3, y_3), and (d) (x_4, y_4).

motor chips arranged opposite to each other to generate reciprocal motion.

6. Conclusion

In this paper, an electrostatic actuator with low energy consumption was powered by a 7.5 mm × 7.5 mm silicon photovoltaic cell with an output voltage of 60 V. With the proper driving waveforms for large displacements, the generated force of the electrostatic inchworm motor chip was enough to actuate the leg of the microrobot. In the future, the authors will design a millimeter-scale locomotive robot with silicon-PV-cell-driven electrostatic inchworm motors. Additionally, the electrostatic inchworm motor chip requires a durability test to investigate the device repeatability.

Acknowledgment

This work was supported by JSPS KAKENHI Grant Number JP18K04060. Also, part of this research was supported by Amano Institute of Technology Public Interest Incorporated Foundation. Fabrication of the microrobot was supported by the Research Center for Micro Functional Devices, Nihon University. Fabrication of the inchworm motors was supported by the UC Berkeley Marvell Nanofabrication Laboratory. The authors would like to acknowledge the Berkeley Sensor and Actuator Center and the UC Berkeley Swarm Lab for their continued support. VLSI Design and Education Center (VDEC), the University of Tokyo (UTokyo), and Phenitec Semiconductor are acknowledged for CMOS-SOI wafer fabrication. The Japanese Ministry of Education, Sports, Culture, Science and Technology (MEXT) is acknowledged for financial support through Nanotechnology Platform to UTokyo VDEC used for the PV cell postprocess. The authors would like to thank Enago (www.enago.jp) for the English language review.

References

[1] T. Ebefors, J. U. Mattsson, E. Kälvesten, and G. Stemme, "A WALKING SILICON MICRO-ROBOT," Proc. of the 10th Int. Conference on Solid-State Sensors and Actuators, Sendai, Japan, pp. 1202–1205, 1999.

[2] S. Hollar, A. Flynn, C. Bellew, and K. S. J. Pister, "Solar powered 10 mg silicon robot," Proc. of the IEEE The Sixteenth Annual International Conference on Micro Electro Mechanical Systems, Kyoto, Japan, pp. 706–711, 2002.

[3] J. Ryu, Y. Jeong, Y. Tak, B. Kim, B. Kim, and J. Park, "A ciliary motion based 8-legged walking micro robot using cast IPMC actuators," Proceedings of 2002 International Symposium on Micromechatronics and Human Science, pp. 85–91, 2002.

[4] B. R. Donald, C. G. Levey, C. D. McGray, I. Paprotny, and D. Rus, "An Untethered, Electrostatic, Globally Controllable MEMS Micro-Robot," Journal of Microelectromechanical Systems, Vol. **15**, No. 1, pp. 1–15, 2006.

[5] M. A. Hoover, E. Steltz, and S. R. Fearing, "RoACH: An autonomous 2.4 g crawling hexapod robot," In Proceedings of the 2008 IEEE/RSJ International Conference on Intelligent Robots and Systems, Nice, France, 22–26 September, pp. 26–33, 2008.

[6] S. Kernbach and O. Kernbach, "Collective energy homeostasis in a large-scale microrobotic swarm," Robotics and Autonomous Systems, Vol. **59**, pp. 1090–1101, 2011.

[7] R. J. Wood, B. Finio, M. Karpelson, K. Ma, N. O. Pérez-Arancibia, P. S. Sreetharan, H. Tanaka, and J. P. Whitney, "Progress on "Pic," Air Vehicles," The International Journal of Robotics Vol. **31**, No. 11, pp. 1292–1302, 2012.

[8] B. R. Donald, C. G. Levey, I. Paprotny, and D. Rus,

"Planning and control for microassembly of structures composed of stress-engineered MEMS microrobots," The International Journal of Robotics Research Vol. **32**, No. 2, pp. 218–246, 2013.

[9] M. Rubenstein, A. Cornejo, and R. Nagpal, "Programmable self-assembly in a thousand-robot swarm," Science 15 Aug 2014: Vol. **345**, Issue 6198, pp. 795–799, 10.1126/science.1254295

[10] J. Qu and K. R. Oldham, "Multiple-Mode Dynamic Model for Piezoelectric Micro-Robot Walking," ASME. International Design Engineering Technical Conferences and Computers and Information in Engineering Conference, Volume 4: 21st Design for Manufacturing and the Life Cycle Conference; 10th International Conference on Micro- and Nanosystems 2016, :V004T08A023, 10.1115/DETC2016-59621.

[11] D. Vogtmann, R. S. Pierre, and S. Bergbreiter, "A 25 MG MAGNETICALLY ACTUATED MICROROBOT WALKING AT > 5 BODY LENGTHS/SEC," Proc. of the IEEE 30th International Conference on Micro Electro Mechanical Systems, Las Vegas, NV, USA, 2017, pp. 179–182, DOI: 10.1109/MEMSYS.2017.7863370.

[12] J. Rahmer, C. Stehning, and B. Gleich, "Spatially selective remote magnetic actuation of identical helical micromachines," Sci. Robot. 2017 2, eaal2845, 10.1126/scirobotics.aal2845.

[13] J. J. Abbott, Z. Nagy, F. Beyeler, and B. J. Nelson, "Robotics in the Small, Part I: Microbotics," IEEE Robotics & Automation Magazine, Vol. **14**, No. 2, pp. 92–103, 2007, 10.1109/MRA.2007.380641.

[14] K. Cho and R. Wood, "Biomimetic robots," Springer International Publishing, Cham, Switzerland, Chap. 23, 2016, ISBN: 978-3-319-32552-1.

[15] R. S. Fearing, "Powering 3 Dimensional Microrobots: Power Density Limitations," Proc. of the IEEE International Conference on robotics and automation, Tutorial on Micro Mechatronics and Micro Robotics. 1998.

[16] D. J. Bell, T. J. Lu, N. A. Fleck, and S. M. Spearing, "MEMS actuators and sensors: observations on their performance and selection for purpose," Journal of Micromechanics and Microengineering, Vol. **15**, No. 7, pp. S153–S164, 2005, 10.1088/0960-1317/15/7/022.

[17] K. Saito, K. Maezumi, Y. Naito, T. Hidaka, K. Iwata, Y. Okane, H. Oku, M. Takato, and F. Uchikoba, "Neural Networks Integrated Circuit for Biomimetics MEMS Microrobot Robotics," Vol. **3**, pp. 235–246, 2014, 10.3390/robotics3030235.

[18] D. Tanaka, Y. Uchiumi, S. Kawamura, M. Takato, K. Saito, and F. Uchikoba, "Four-leg independent mechanism for MEMS microrobot. Artificial Life and Robotics," September 2017, Vol. **22**, Issue 3, pp 380–384, 10.1007/s10015-017-0365-2.

[19] R. Yeh, S. Hollar, and K. S. J. Pister, "Single mask, large force and large displacement electrostatic linear inchworm motors," J. Microelectromech. Syst. Vol. **11**, No. 4, pp. 330–336, 2002, 10.1109/JMEMS.2002.800937.

[20] I. Penskiy and S. Bergbreiter, "Optimized electrostatic inchworm motors using a flexible driving arm," Journal of Micromechanics and Microengineering, Vol. **23**, No. 1, pp. 1–12, 2012, 10.1088/0960-1317/23/1/015018.

[21] D. S. Contreras, D. S. Drew, and K. S. J. Pister, "First steps of a millimeter-scale walking silicon robot," Proc. of the 19th Int. Conference on Solid-State Sensors, Actuators and Microsystems, Kaohsiung, Taiwan, 2017.

[22] I. Mori, M. Kubota, E. Lebrasseur, and Y. Mita, "Remote power feed and control of MEMS with 58 V silicon photovoltaic cell made by a CMOS post-process dry release and device isolation method," Symposium on Design, Test, Integration & Packaging of MEMS/MOEMS (DTIP2014), April 1–4, Cannes, France, 10.1109/DTIP.2014.7056670.

[23] Y. Takeshiro, Y. Okamoto, and Y. Mita, "Mask-programmable on-chip photovoltaic cell array," Proc. of the Power MEMS 2017, November 14-17, Kanazawa, Japan, pp. 596–597.

Ken Saito
Daniel S. Contreras
Yudai Takeshiro
Yuki Okamoto
Satoshi Hirao
Yuya Nakata
Taisuke Tanaka
Satoshi Kawamura
Minami Kaneko
Fumio Uchikoba
Yoshio Mita
Kristofer S. J. Pister